AMERICAN SOCIETY FOR MICROBIOLOGY | Antimicrobial Agents and Chemotherapy

Clofazimine Biocrystal Accumulation in Macrophages Upregulates Interleukin 1 Receptor Antagonist Production To Induce a Systemic Anti-Inflammatory State

Gi S. Yoon,[a] Rahul K. Keswani,[a] Sudha Sud,[a] Phillip M. Rzeczycki,[a] Mikhail D. Murashov,[a] Tony A. Koehn,[a] Theodore J. Standiford,[b] Kathleen A. Stringer,[c] Gus R. Rosania[a]

Department of Pharmaceutical Sciences, College of Pharmacy,[a] Department of Internal Medicine, University of Michigan Medical Center,[b] and Department of Clinical Pharmacy, College of Pharmacy,[c] University of Michigan, Ann Arbor, Michigan, USA

Clofazimine (CFZ) is a poorly soluble antibiotic and anti-inflammatory drug indicated for the treatment of leprosy. In spite of its therapeutic value, CFZ therapy is accompanied by the formation of drug biocrystals that accumulate within resident tissue macrophages, without obvious toxicological manifestations. Therefore, to specifically elucidate the off-target consequences of drug bioaccumulation in macrophages, we compared the level of inflammasome activation in CFZ-accumulating organs (spleen, liver and lung) in mice after 2 and 8 weeks of CFZ treatment when the drug exists in soluble and insoluble (biocrystalline) forms, respectively. Surprisingly, the results showed a drastic reduction in caspase 1 and interleukin-1β (IL-1β) cleavage in the livers of mice treated with CFZ for 8 weeks (8-week-CFZ-treated mice) compared to 2-week-CFZ-treated and control mice, which was accompanied by a 3-fold increase in hepatic IL-1 receptor antagonist (IL-1RA) production and a 21-fold increase in serum IL-1RA levels. In the lung and spleen, IL-1β cleavage and tumor necrosis factor alpha expression were unaffected by soluble or biocrystal CFZ forms. Functionally, there was a drastic reduction of carrageenan- and lipopolysaccharide-induced inflammation in the footpads and lungs, respectively, of 8-week-CFZ-treated mice. This immunomodulatory activity of CFZ biocrystal accumulation was attributable to the upregulation of IL-1RA, since CFZ accumulation had minimal effect in IL-1RA knockout mice or 2-week-CFZ-treated mice. In conclusion, CFZ accumulation and biocrystal formation in resident tissue macrophages profoundly altered the host's immune system and prompted an IL-1RA-dependent, systemic anti-inflammatory response.

Clofazimine (CFZ) is an antimycobacterial agent listed in the World Health Organization's List of Essential Medicines that has been in use as part of the standard treatment of leprosy since the 1960s (1, 2). The number of leprosy cases has drastically dropped from 12 million/year in 1981 to 216,000/year in 2013 (3), a testament to the effectiveness of CFZ, which has gained considerable attention recently as part of a treatment regimen for drug-resistant tuberculosis (4–6). The efficacy of oral CFZ against leprosy is due, in part, to its well-documented anti-inflammatory activity (2). However, CFZ's mechanism of anti-inflammatory action and atypical pharmacokinetic properties are not well understood, and its high oral bioavailability and poor solubility leads to significant bioaccumulation in tissues (7).

In previous studies, it has been shown that following prolonged oral administration of CFZ, the drug massively bioaccumulates as intracellular biocrystals in resident tissue macrophages (8–12). Therefore, it is natural to assume that this bioaccumulation phenomenon contributes to the drug's toxicity, whereas the soluble form of CFZ, which circulates and partitions to and from the different organs, is responsible for CFZ's mechanism of action. Indeed, insoluble particles and crystals that accumulate in macrophages under various pathological conditions are known to activate immune signaling pathways that lead to caspase 1 (Casp 1) activation and increased interleukin-1β (IL-1β) secretion (13–16). This so-called "inflammasome" activation pathway is often associated with many downstream pathological changes, as has been shown by the accumulation of cholesterol monohydrate crystals in atherosclerosis (13), monosodium urate crystals in gout (14), and inhaled foreign particles in the case of asthma and other chronic inflammatory lung diseases (15, 16).

In spite of its bioaccumulation, several clinical trials have established CFZ as a potentially useful therapeutic agent for treating a variety of chronic inflammatory diseases (17–22). Furthermore, *in vitro* studies have shown that intracellular CFZ biocrystals dampen proinflammatory pathways while enhancing anti-inflammatory signals (23).

In order to distinguish between the potential adverse effects of insoluble drug biocrystals from those of the soluble molecules, we designed an experimental strategy to compare how the accumulation of insoluble drug biocrystals might influence the immune signaling response of macrophages in live mice. We reasoned that macrophages exposed to the soluble form of CFZ (after 2 weeks of treatment) may behave differently from those that are exposed to its biocrystalline form (after 8 weeks of treatment). Accordingly, we tested the specific hypothesis that CFZ biocrystals that accumulate in resident tissue macrophages can modulate (or activate)

Received 2 February 2016 **Returned for modification** 28 February 2016
Accepted 17 March 2016

Accepted manuscript posted online 28 March 2016

Citation Yoon GS, Keswani RK, Sud S, Rzeczycki PM, Murashov MD, Koehn TA, Standiford TJ, Stringer KA, Rosania GR. 2016. Clofazimine biocrystal accumulation in macrophages upregulates interleukin 1 receptor antagonist production to induce a systemic anti-inflammatory state. Antimicrob Agents Chemother 60:3470–3479. doi:10.1128/AAC.00265-16.

Address correspondence to Gus R. Rosania, grosania@umich.edu.

Supplemental material for this article may be found at http://dx.doi.org/10.1128/AAC.00265-16.

these cells' inflammatory signaling pathways *in vivo* that lead to systemic changes in the inflammatory response. By assessing tumor necrosis factor alpha (TNF-α) and IL-1 receptor antagonist (IL-1RA) expression, as well as Casp 1 and IL-1β maturation, in the vital organs and blood of CFZ-treated mice, our results demonstrate that CFZ biocrystals in macrophages, but not the soluble form, is specifically associated with an IL-1RA-mediated anti-inflammatory response.

MATERIALS AND METHODS

Reagents. Anti-caspase 1 and anti-IL-1β antibodies were purchased from Thermo Pierce (Rockford, IL) and Novus Biologicals (Littleton, CO), respectively. Anti-F4/80 and anti-CD68 antibodies were purchased from Abcam (Cambridge, MA). Anti-actin antibody and lipopolysaccharide (LPS; from *E. coli* O55:B5) were purchased from Sigma (St. Louis, MO).

Mice clofazimine treatment. Clofazimine (CFZ; Sigma-Aldrich, catalog no. C8895) was prepared in sesame oil (Shirakiku, Japan, or Roland, China) and Powdered Lab Diet 5001 (PMI International, Inc., St. Louis, MO) and orally administered to wild-type (WT) C57BL/6 mice or IL-1RA knockout mice (4 to 5 weeks old; Jackson Laboratory, Bar Harbor, ME) for up to 8 weeks *ad libitum* as previously described (8, 24). Control mice were fed with the same diet without CFZ. The animal protocol was approved by the University of Michigan's Animal Care and Use Committee in accordance with the National Institutes of Health guidelines (UCUCA, no. PRO00005542).

Carrageenan footpad edema test. Footpad edema in response to carrageenan (CAR; Sigma) injection was measured in CFZ-treated and control mice as previously described (25). In IL-1RA knockout (KO) mice, these experiments were performed at 6 weeks and not at 8 weeks because the IL-1RA KO mice weighed less than the WT mice and their livers were smaller (see Fig. S4 in the supplemental material). In brief, the volume of each hind paw was measured before and after the intraplantar injection of 30 μl of 2% CAR (60 μg per paw) in phosphate-buffered saline (PBS) or an equal volume of PBS in the contralateral paw. Paw swelling was measured at 4 and 48 h after injection, after which the animals were euthanized by exsanguination while deeply anesthetized with an intraperitoneal injection of ketamine (100 mg/kg) and xylazine (10 mg/kg), and the skin tissues of the plantar region were harvested for cytokine assay (see the Materials and Methods in the supplemental material).

Acute lung injury and infrared pulse oximetry. Since C57BL/6 mice are relatively resistant toward a single dose of intratracheal (i.t.) LPS instillation (26), two i.t. injections of LPS (16 mg/kg; 50 μl) were administered, one on day 0 and the second on day 3. Briefly, mice treated with CFZ for 8 weeks (8-week-CFZ-treated mice) and control mice were anesthetized using intraperitoneal injections of xylazine (50 mg/kg) and ketamine (5 mg/kg). Under direct visualization of the vocal cords using an otoscope, either LPS or an equivalent volume of PBS in a 1-ml syringe attached to an oral gavage needle (22G) was instilled into the lungs via the oral route. The mouse was then placed in a temperature-controlled cage (37°C) for recovery from anesthesia.

The general health status of each PBS/LPS-instilled mice was monitored by measuring body weight and rectal temperature (microprobe thermometer; Physitemp Instruments, Clifton, NJ), and cardiopulmonary function (arterial oxygen saturation, respiratory rate, heart rate, and pulse distention) was monitored using MouseOx with a collar clip sensor (Starr Life Sciences Corp., Oakmont, PA) as previously described (27, 28). In brief, 1 day before i.t. instillations (day −1), the hair around the neck of each mouse was removed using Nair (Church & Dwight, Princeton, NJ) to enable data acquisition using the collar clip sensor. The next day (day 0), immediately prior to the first LPS/PBS dose, and every 24 h afterward until day 6, the body weight, temperature, and MouseOx readings were recorded. MouseOx data were acquired by very brief anesthesia of the mouse using 5% isoflurane to facilitate the placement of the collar clip sensor. The mouse was then placed in an enclosed chamber with ambient light and allowed to acclimatize for 5 min, at which point the animals had recovered normal activities and physiological readings. Arterial oxygen saturation, respiratory rate, heart rate, and pulse distention measurements were then simultaneously recorded for 6 min (15 readings/s), and any errors caused by motion during recording were excluded, after which the mean value of each parameter was used for further data analysis.

Terminal endpoint assessment. To objectively assess LPS-induced mortality, we used a multiparametric scoring system that relied on the daily changes in vital signs associated with inflammatory injury progression and mortality, which included arterial oxygen saturation (27), body weight, and temperature (29, 30). First, the percent change from baseline (day 0) in arterial oxygen saturation, body weight, and temperature in each mouse caused by i.t. instillation of PBS/LPS were measured and calculated daily until day 6 after instillation. These data were then used in a vector equation to calculate the distance between each LPS-treated mouse and the mean of the PBS-treated mice to assess the terminal endpoint for each LPS-instilled mouse (see Materials and Methods in the supplemental material). CFZ-treated and control mice were calculated separately, and LPS-instilled mice that scored a total of 18 or higher were determined as terminal, since these mice also displayed severe signs of sickness evidenced by impaired mobility, lack of grooming, hunched posture, and muscle weakness that could be felt while handling the mice. These mice were immediately euthanized with ketamine-xylazine (100 mg/kg, 10 mg/kg) and the bronchoalveolar lavage (BAL) fluid and lungs were harvested for cellular and biochemical analysis (see below). Remaining mice that did not reach terminal endpoint were all euthanized on day 6 after PBS/LPS instillation.

Cytokine measurements. The harvested organs (liver, spleen, lungs, and kidneys) and footpads designated for cytokine assays were cut and homogenized by sonication (2-s pulses repeated five times on ice, level 5; Fisher model 100) in radioimmunoprecipitation assay buffer (Sigma) with added protease inhibitors (Halt protease and phosphatase inhibitor cocktail and 0.5 M EDTA; Thermo Pierce, Rockford, IL). After centrifugation (18,000 × *g*, 15 min, 4°C), the supernatants were assayed for IL-1β, IL-1RA, and TNF-α by enzyme-linked immunosorbent assay (ELISA; Duoset; R&D Systems, Minneapolis, MN) in duplicate wells according to the manufacturer's instructions. Cytokines in the BAL were measured after the removal of the cells. Albumin was assayed by ELISA (Innovative Research, Novi, MI). The cytokine concentrations were expressed (i) as pico-, nano-, or micrograms per milligram of protein for the organs, (ii) as pico-, nano-, or micrograms of paw weight, or (iii) as pico- or micrograms per milliliter of BAL fluid.

Mouse BAL fluid harvesting, immunohistochemistry and imaging, and SDS-PAGE and Western blotting. The mouse BAL fluid harvesting, immunohistochemistry and imaging, and SDS-PAGE and Western blotting procedures are described in the supplemental material.

Data processing and statistics. All data are expressed as means ± the standard deviations (SD). For multiple comparisons, statistical analysis was performed with one-way analysis of variance (ANOVA) and Tukey's post *hoc* comparisons. For two-group comparisons, an unpaired Student *t* test was used. All statistical analyses employed the Sigmaplot version 13 (Systat Software, San Jose, CA) software and $P \leq 0.05$ was considered statistically significant.

RESULTS

CFZ crystallization and bioaccumulation in the liver occurs after 2 weeks. During the first 2 weeks of CFZ treatment, CFZ-associated diffuse red staining was present throughout the liver (Fig. 1A, brightfield). However, by 4 weeks, CFZ accumulated in the biocrystalline form. At 8 weeks, red CFZ biocrystals were evident throughout the liver (Fig. 1A, top panel). Taking advantage of solvatochromic changes in the fluorescent excitation and emission spectra of CFZ (31, 32), fluorescence microscopy enabled *in vivo* detection of the soluble and biocrystalline forms of CFZ. After 2 weeks of CFZ treatment, the drug was mostly present in the soluble form with its fluorescence mostly detectable in the FITC

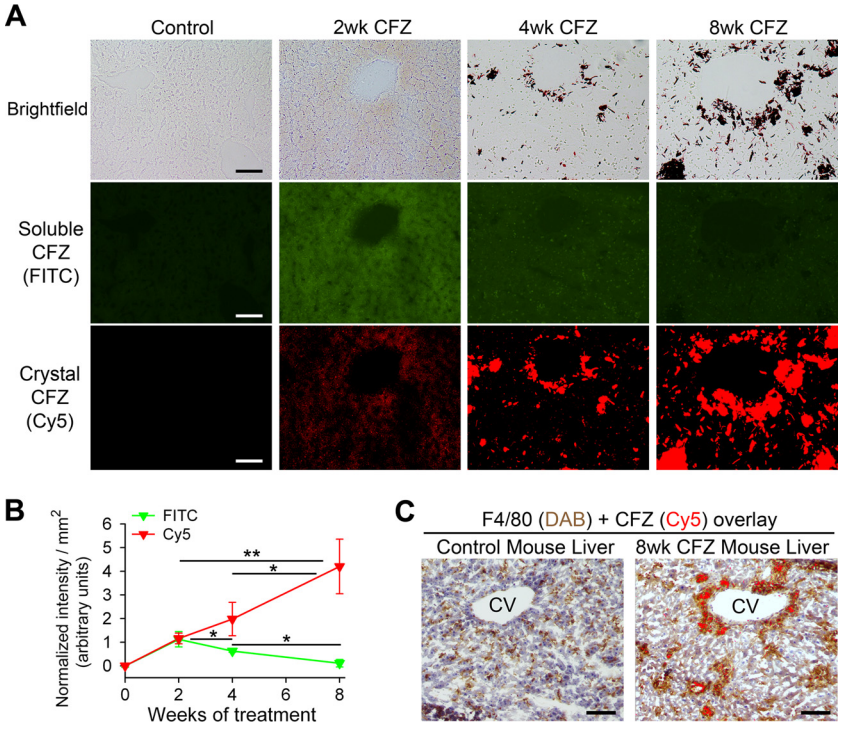

FIG 1 CFZ bioaccumulation and crystal formation in the liver occurs after 2 weeks. (A) Representative bright-field and fluorescence (FITC for soluble CFZ and Cy5 for crystalline CFZ) images of liver sections from control mice and mice treated with CFZ for 2, 4, and 8 weeks. Scale bar, 50 μm. (B) Fluorescence intensity values (FITC and Cy5 channels) of liver sections from control and CFZ-treated mice. Baseline (0 week) intensity values of controls were subtracted from CFZ-treated sections. The data are the means ± the SD of results from three to four images/time point. One-way ANOVA was used to compare fluorescence intensity between time points and $P \leq 0.05$ was considered statistically significant. *, $P \leq 0.05$; **, $P \leq 0.01$. (C) F4/80 (DAB) immunohistochemistry of a representative liver section from an 8-week-CFZ-treated mouse in which CFZ crystals (Cy5) are sequestered inside F4/80$^+$ macrophages. CV, central vein. Scale bar, 100 μm.

channel (Fig. 1A, fluorescein isothiocyanate [FITC] and Cy5 panels; Fig. 1B). At later time points, the fluorescence signal in the FITC channel declined, while the fluorescence signal in the Cy5 channel increased, indicating the relative accumulation of the biocrystalline form (Fig. 1A and B). By 8 weeks, most of the fluorescence signal was detectable in the Cy5 channel (Fig. 1 A and B), indicating that CFZ was present almost entirely in biocrystalline form. Immunohistochemistry of 8-week-CFZ-treated liver sections showed that CFZ biocrystals are sequestered inside F4/80-positive macrophages (Fig. 1C). Such targeted accumulation of CFZ biocrystals was also detected in other organs such as CD68$^+$ alveolar macrophages (see Fig. S1 in the supplemental material), and F4/80$^+$ splenic macrophages (8, 31).

CFZ biocrystal formation in the liver downregulates Casp 1/IL-1β processing while enhancing IL-1RA expression. Intracellular crystals, such as those formed by cholesterol or uric acid, have been implicated in the activation of the NLRP3-Casp 1 inflammasome, which plays a major role in the pathogenesis of chronic inflammatory disorders (14, 33, 34). The uptake of other nano- and microparticles has also been reported to cause inflammasome activation in macrophages (35–37). Therefore, to assess whether the bioaccumulation of CFZ crystals leads to activation of the inflammasome, we measured and compared cleaved Casp 1 and IL-1β in organs that bioaccumulate CFZ—i.e., the liver, spleen, and lungs—and kidneys, that do not accumulate CFZ, after 2 and 8 weeks of either CFZ or control treatment. Two weeks of CFZ exposure resulted in only moderate cleavage of hepatic Casp 1 and IL-1β (Fig. 2A, left panel, and Fig. 2B). However, by 8 weeks, Casp 1 and IL-1β cleavage was significantly reduced by CFZ treatment (Fig. 2A, right panel, and Fig. 2B); IL-1β levels in the spleen, lung, and kidneys did not change (see Fig. S2 in the supplemental material). The expression of the proinflammatory cytokine, TNF-α, was unchanged by CFZ at both 2 and 8 weeks (Fig. 2C), except in the liver, where it was decreased at 2 weeks compared to control livers.

Similar to previous observations (8), we found that after 8 weeks of oral administration CFZ caused a major upregulation of IL-1RA expression in CFZ biocrystal-accumulating organs, such as the spleen, the lungs, and especially the liver, which increased by 3-fold (Fig. 2D). IL-1RA levels in the kidney were unaffected (Fig. 2D). In contrast, after 2 weeks of oral CFZ administration there were more modest increases in only the spleen and lungs, while the liver was unaffected (Fig. 2D). Since the liver is known to be the major source of circulating IL-1RA (38, 39), we observed a corresponding increase in serum IL-1RA levels in CFZ-treated mice at 8 weeks but not at 2 weeks (Fig. 2E). Under all conditions, neither TNF-α nor IL-1β was detected in the serum. In aggregate, these findings suggest that crystallized CFZ, which is evident after 8 weeks of CFZ administration, decreased the activation of the inflammasome *in vivo*. In parallel with this decline, crystallized CFZ induced an upregulation of endogenous IL-1RA.

Systemic CFZ bioaccumulation and crystallization dampens CAR-mediated acute footpad inflammation. To test the physiological impact of the CFZ-induced serum IL-1RA levels, we tested

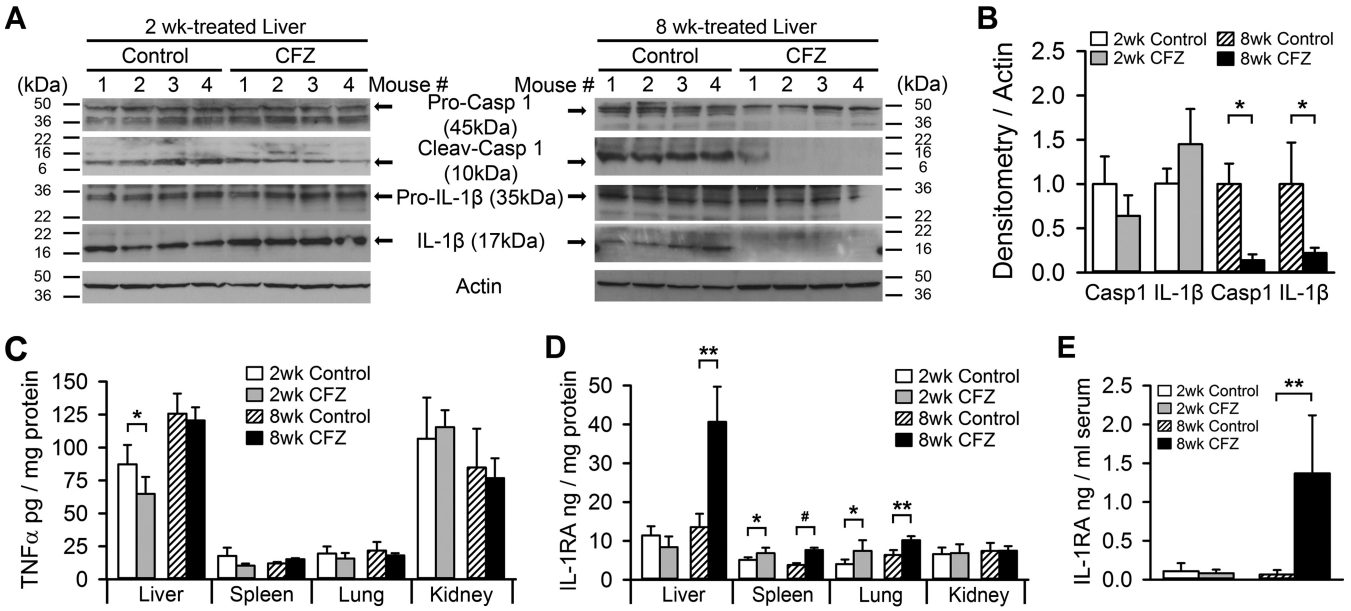

FIG 2 CFZ bioaccumulation reduces Casp 1 and IL-1β cleavage levels in the liver but increases IL-1RA expression. (A) Representative Western blots of liver homogenates showing that Casp 1 and IL-1β cleavage was not altered by 2 weeks of CFZ treatment but that 8 weeks of treatment reduced the detection of Casp 1 and IL-1β cleavage. (B) Densitometry of cleaved Casp 1 and IL-1β protein in 2- and 8-week-treated liver blots, normalized to actin ($n = 4$). Hepatic Casp 1 and IL-1β cleavage were reduced by 86 and 78%, respectively, in 8-week-CFZ-treated mice. (C) The levels of TNF-α in the spleen, lungs, and kidneys were unchanged by CFZ treatment, but there was a significant decrease in liver TNF-α from 2-week-CFZ-treated mice ($n = 4$ to 5). (D) The organs that bioaccumulate CFZ crystals—liver, spleen, and lung—displayed increased IL-1RA expression, whereas the kidney, which does not accumulate CFZ, did not show changes in IL-1RA expression ($n = 4$ to 5). (E) Serum IL-1RA levels were unchanged after 2 weeks but were increased 21-fold after 8 weeks of CFZ treatment. The serum TNF-α and IL-1β levels were below the limit of detection of the assay ($n = 6$). *, $P \leq 0.05$; **, $P \leq 0.01$; #, $P \leq 0.001$. Data are means ± the SD, and an unpaired Student *t* test was used to compare control mice versus CFZ-treated mice.

the acute inflammatory response of CFZ-treated mice by using a well-established footpad injury model (25). The paws of 8-week-CFZ-treated mice displayed strikingly reduced swelling at 48 h after the injection of CAR compared to the paws of untreated CAR-injected mice (Fig. 3A). Paw volume measurements showed that there was a significant reduction (57%) in footpad swelling as early as 4 h after the injection of CAR in 8-week-CFZ-treated mice compared to control mice, and the animals continued to exhibit reduced swelling over the 48-h study period (Fig. 3B). CAR-induced increases in footpad IL-1β and TNF-α levels were dramatically reduced by 8-week-CFZ treatment (Fig. 3C and D). In contrast to the 8-week-treated mice, 2-week-CFZ-treated mice produced only a modest reduction in paw swelling compared to control mice (Fig. 3E and F). The IL-1β and TNF-α levels in footpad homogenates from these animals were similar in both CFZ-treated and control mice at 48 h (Fig. 3G and H). Accordingly, these results suggest that the accumulation of CFZ biocrystals modulated the immune response to profoundly dampen CAR-induced footpad inflammation, and this action is not evident for the soluble form of the drug after 2 weeks of treatment.

CFZ biocrystals dampen the acute inflammatory response in the footpad by increasing blood IL-1RA. IL-1RA is known to be an early-acting acute-phase anti-inflammatory cytokine (38), and circulating IL-1RA has been reported to dampen a broad spectrum of inflammatory conditions by inhibiting the activity of IL-1β at the site of injury (40, 41). Therefore, we hypothesized that the anti-inflammatory response observed after 8 weeks of CFZ treatment may be mediated by increased serum IL-1RA concentrations, which are not evident after 2 weeks of CFZ treatment (Fig. 2E). Detection of serum IL-1RA in 2-week-CFZ-treated and control mice showed comparable IL-1RA levels before (0 h) and after (48 h) CAR injection (Fig. 4A). However, serum IL-1RA levels in 8-week-CFZ-treated mice rapidly declined 4 h after CAR injection (Fig. 4B). After 48 h, IL-1RA returned to similar levels in the plasma of control and 8-week-CFZ-treated mice (Fig. 4B). For all mice, the plasma levels of TNF-α and IL-1β were below the detection limit of ELISAs (15 pg/ml). These results suggest that increased circulating IL-1RA levels associated with CFZ bioaccumulation and crystallization could be responsible for the anti-inflammatory activity observed in 8-week-CFZ-treated mice.

In order to test the possibility that elevated IL-1RA expression mediates the anti-inflammatory activity of CFZ after crystal formation, we administered oral CFZ to age-matched IL-1RA KO and WT mice and then subjected the animals to the CAR footpad injury model. IL-1RA KO mouse livers also increased in weight to an extent similar to that of WT mice after 6 weeks of CFZ treatment (see Fig. S3B in the supplemental material). Also, IL-1RA KO mice formed and accumulated CFZ biocrystals in the liver at a level similar to WT animals without noticeable differences in crystal shape or Cy5 fluorescence intensity (see Fig. S3C and D in the supplemental material). Remarkably, the anti-inflammatory action of CFZ bioaccumulation was greatly diminished in IL-1RA KO mice, since CFZ-treated and CAR-injected IL-1RA KO mice displayed similar swelling compared to untreated and CAR-injected IL-1RA KO mice (Fig. 4C and D, right panels). In the CFZ-treated WT mice, we observed significantly reduced CAR-induced swelling compared to control mice at 4 and 48 h postinjury (Fig. 4C and D, WT panels). As expected, the footpad IL-1β and TNF-α

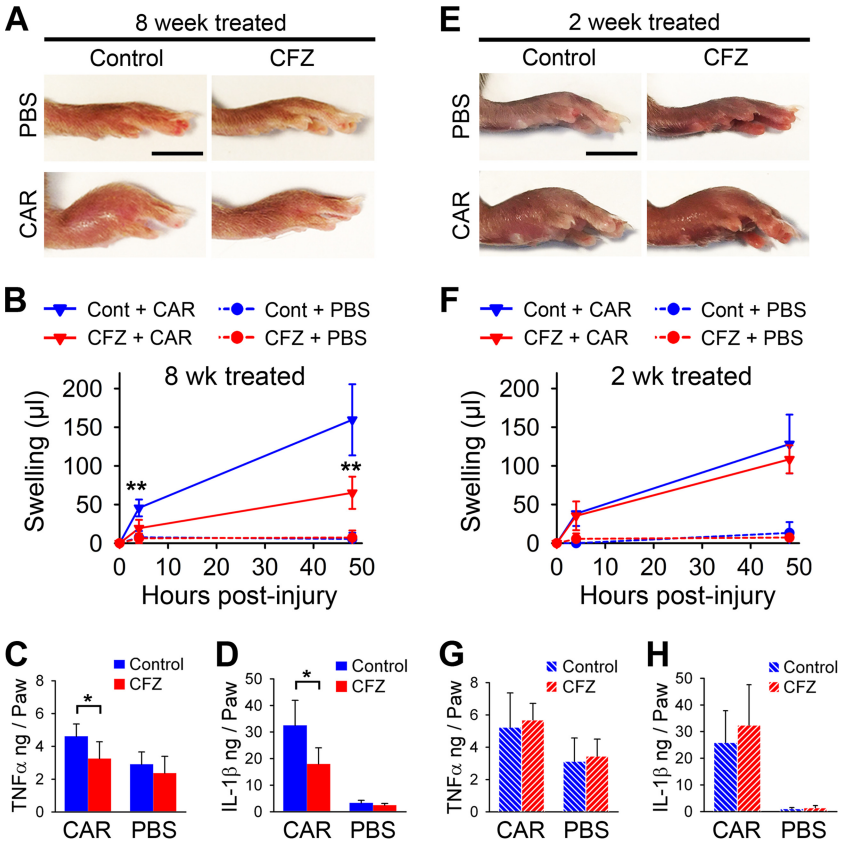

FIG 3 Systemic CFZ bioaccumulation and crystal formation dampens CAR-induced inflammatory response in the mouse footpad. (A) Representative photographs of paws 48 h after CAR or PBS footpad injection show markedly reduced paw swelling in 8-week-CFZ-treated mice compared to control mice. Scale bar, 5 mm. (B) Paw swelling, as measured by foot volume, was reduced on average by 57% as early as 4 h after CAR injection in 8-week-CFZ-treated mice compared to control mice and was sustained through 48 h. The footpad homogenate cytokine levels of IL-1β (C) and TNF-α (D) were reduced in 8-week-CFZ-treated mice at 48 h compared to untreated and injured paws. (E and F) Representative photographs of paws 48 h after CAR or PBS footpad injection in 2-week-CFZ-treated or control mice (E), which resulted in only a minor reduction in swelling at 4 and 48 h (F). Scale bar, 5 mm. (G and H) Associated footpad homogenate TNF-α (G) and IL-1β (H) levels were unchanged. PBS-injected paws did not show any difference in cytokine expression between CFZ-treated or control paws. Data are means ± the SD of $n = 5$ to 6/experiment. An unpaired Student t test was used to compare control versus CFZ-treated mice. *, $P \leq 0.05$; **, $P \leq 0.01$.

levels were significantly reduced in WT CFZ-treated and CAR-injected mice compared to WT untreated and CAR-injected mice (Fig. 4E). However, the IL-1β and TNF-α levels were comparable in the CAR-injected IL-1RA KO mice with or without CFZ treatment (Fig. 4F). IL-1RA KO mice with or without CFZ treatment showed higher cytokine levels than the control WT mice after CAR injection (Fig. 4E versus Fig. 4F), but the footpad swelling was similar (Fig. 4D). These results are consistent with CFZ bioaccumulation exerting a systemic anti-inflammatory action via the elevation of blood IL-1RA levels.

CFZ bioaccumulation enhances resistance to acute lung injury and improves mouse survival. Given the massive bioaccumulation of CFZ observed in the lungs, we proceeded to determine whether the presence of CFZ biocrystals in these organs may sensitize mice to a sublethal proinflammatory injury. Although CFZ treatment and bioaccumulation did cause some physiological changes, these changes were within ranges of normal physiological readings and overall mouse health was normal (see Table S1 in the supplemental material).

To determine whether CFZ bioaccumulation induced a latent proinflammatory state in mouse lungs, a sublethal dose of LPS (16 mg/kg) was delivered i.t. to control and CFZ-treated mice. Strikingly, CFZ-treated mice were highly resistant to LPS-induced acute lung injury, with a 92% survival rate compared to the 42% survival rate of control mice (Fig. 5A). The difference in the arterial oxygen saturation levels between control and CFZ-treated mice was more prominent after the second LPS injection. CFZ-treated mice displayed significantly higher arterial oxygen levels at days 5 and 6 than control mice because most control mice experienced levels of hypoxia that required euthanasia, indicating that control mice showed progressive deterioration in lung function compared to CFZ-treated mice (see Fig. S4A in the supplemental material). Paralleling the impaired lung function, LPS-injected control mice lost weight more rapidly than CFZ-treated mice, such that six control mice lost >15% of their body weight compared to a similar weight loss in one CFZ-treated mouse (see Fig. S4B in the supplemental material). Both control and CFZ-treated LPS-injected mice displayed large drops in body temperature one day after LPS injection (days 1 and 4). However, CFZ-treated mice were more resistant to a decline in body temperature after the second injection compared to control mice (day 4) (see Fig. S4C in the supplemental material). CFZ-treated mice also displayed less reduction in heart rate, respiratory rate, and pulse distention after the second LPS injection (see Fig. S4D to F in the supplemental

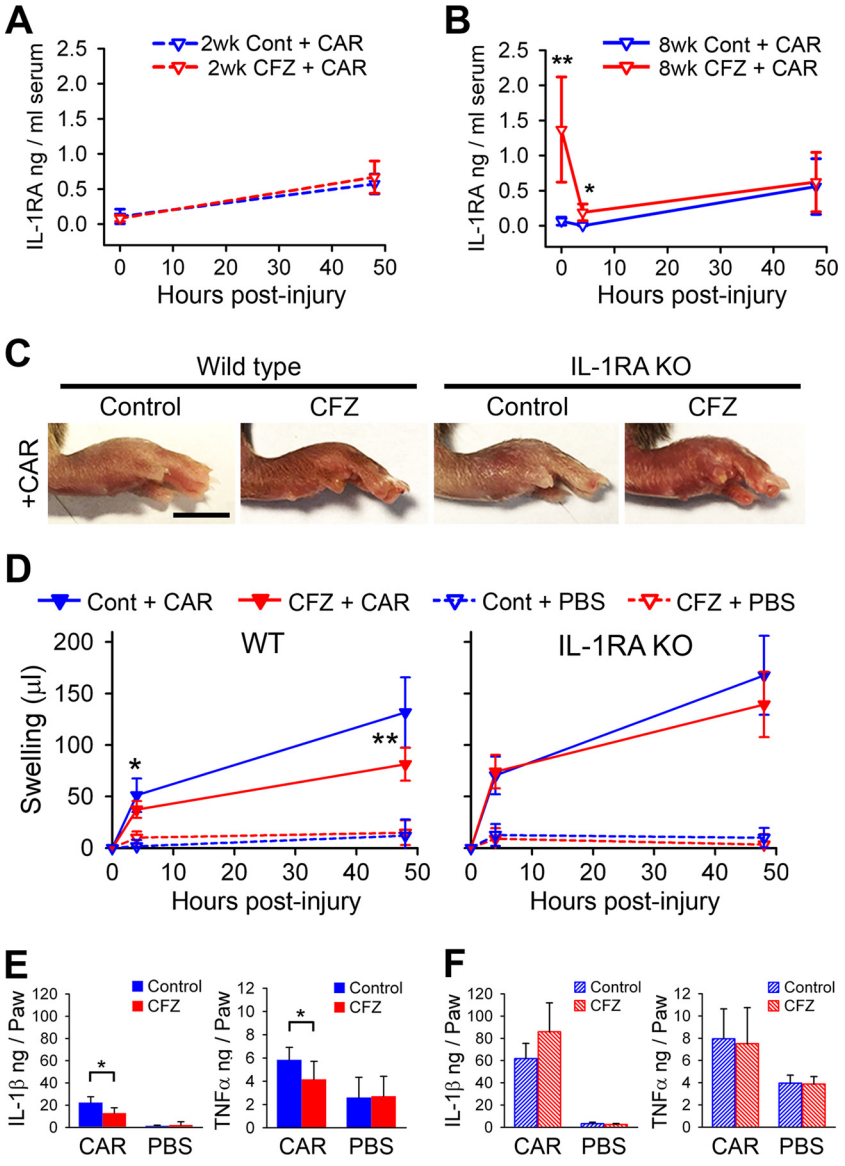

FIG 4 The CFZ-induced dampening of the acute inflammatory response in the CAR footpad model is mediated by circulating IL-1RA. (A) Two-week-CFZ-treated and control wild-type (WT) mice displayed similar serum IL-1RA levels before (0 h) and after (48 h) CAR injection. (B) Serum IL-1RA concentrations were significantly increased after 8 weeks of CFZ treatment compared to controls in WT mice (0 h). CAR injection in 8-week-CFZ-treated mice caused a sharp decline in serum IL-1RA concentrations by 4 h, whereas the levels in control CAR mice remained constant. At 48 h after CAR injection, the serum IL-1RA increased to similar levels in both control and CFZ-treated WT mice (data are means ± the SD of $n = 5$ to 8 animals/group/time point). (C) Representative images of inflamed paws of 6-week-CFZ-treated WT mice and IL-1RA KO mice at 48 h after CAR injection. (D) Footpad swelling, as measured by foot volume, was reduced by 27 and 38% at 4 and 48 h after CAR injection, respectively, in 6-week-CFZ-treated WT mice compared to control WT mice. In IL-1RA KO mice with CFZ treatment, paw swelling was similar at 4 h compared to untreated littermates, and at 48 h, swelling was marginally reduced (17%) compared to untreated IL-1RA KO mice. (E) Footpad homogenate levels of IL-1β and TNF-α were dampened in 6-week-CFZ-treated and CAR-injected WT mice at 48 h compared to control and CAR-injected paws. (F) Footpad homogenate levels of IL-1β and TNF-α were unaffected in 6-week-CFZ-treated and CAR-injected IL-1RA KO mice at 48 h compared to control and CAR-injected paws. Data are the compilation of two separate experiments and are presented as means ± the SD ($n = 7$ to 9). A Student t test was used to compare untreated versus CFZ-treated mice at each time point. *, $P \leq 0.05$; **, $P \leq 0.01$. Scale bar, 5 mm.

material) compared to control mice. Gross lung examination lungs after LPS-induced injury showed a notable reduction of hemorrhaging in CFZ-treated mice compared to control mice (Fig. 5B). Cellular and biochemical analyses of BAL fluid to assess lung injury revealed that CFZ treatment reduced the LPS-induced BAL fluid cell count (Fig. 5C) and reduced the BAL fluid albumin concentrations (Fig. 5D). This CFZ-mediated reduction in lung injury was corroborated by CFZ-induced reductions in LPS-induced levels of BAL fluid TNF-α and IL-1β (Fig. 5E and F). These results demonstrate that CFZ biocrystal accumulation in the lungs did not impair lung function but instead increased resistance to LPS-induced inflammatory lung injury.

DISCUSSION

Previously, CFZ bioaccumulation has been associated with atypical pharmacokinetics, as well as more serious side effects, ranging

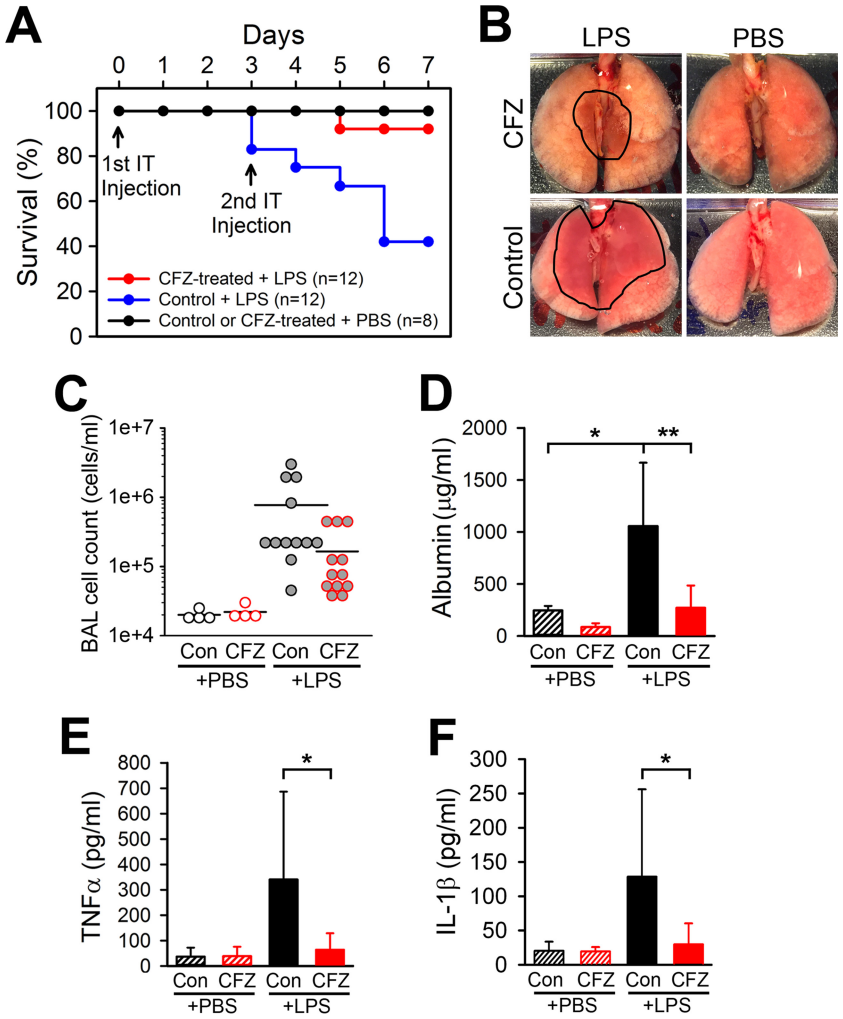

FIG 5 CFZ bioaccumulation enhances resistance to LPS-induced lung injury and improves mouse survival. (A) Kaplan-Meier survival curve showing the 92% survival rate of 8-week-CFZ-treated mice after LPS-induced acute lung injury compared to the 42% survival rate of control mice with LPS-induced injury. (B) A representative photograph shows the gross appearance of the lungs after PBS or LPS injection in control and CFZ-treated mice. Hemorrhaged areas caused by LPS injection are outlined in black lines. (C to F) CFZ treatment reduced LPS-induced increases in the BAL fluid cell count (C), albumin level (D), TNF-α level (E), and IL-1β level (F). The data are the compilation of two separate experiments and are presented as means ± the SD (PBS, $n = 4$; LPS, $n = 12$). One-way ANOVA was used to compare control versus CFZ-treated mice with PBS or LPS injections, and $P \leq 0.05$ was considered statistically significant. *, $P \leq 0.05$; **, $P \leq 0.01$.

from gastrointestinal problems to splenic infarcts (42). Although expecting that CFZ bioaccumulation would lead to an upregulation of proinflammatory signaling pathways in macrophages, we were surprised to find the opposite. Instead, our experimental results indicate that long-term oral administration of CFZ and its sequestration as biocrystals within the macrophages of the lung, the spleen, and especially the liver can dramatically suppress inflammation in peripheral tissues and increase mouse survival in response to acute lung injury. This systemic anti-inflammatory response parallels the accumulation of CFZ biocrystals throughout the animal and is accompanied by elevated IL-1RA levels in these organs and a corresponding boost in IL-1RA levels in serum. Of noteworthy significance, the formation and accumulation of cholesterol monohydrate and monosodium urate crystals have been implicated in the pathogenesis of chronic inflammatory diseases, such as atherosclerosis, nonalcoholic steatohepatitis (NASH) (34), and gout (43). Moreover, other artificial nano- and microparticles, such as silica crystals (37), aluminum salt crystals (44), silver nanoparticles (35), poly(lactide-co-glycolide) (PLG), and polystyrene microparticles (36), have also been reported to cause inflammasome activation in macrophages. At the cellular level, the aforementioned particles or crystals are known to augment Toll-like receptor signaling and activate the NLRP3 inflammasome via lysosomal destabilization, which leads to Casp 1 activation and the production of cleaved IL-1β (13, 14). Therefore, the finding that inflammasome activity was inhibited in the CFZ biocrystal-containing liver, evidenced by the suppression of Casp 1 activation and mature IL-1β processing, was unexpected. Moreover, the presence of CFZ biocrystals in the lung, spleen, or liver did not alter the TNF-α levels, a finding consistent with a lack of proinflammatory signaling.

These results prompt us to question whether CFZ bioaccumulation is an inherently toxic phenomenon. It is well known that soluble CFZ is toxic *in vitro*, with a 50% inhibitory concentration

of approximately 5 μM, whereas the insoluble crystalline form of CFZ that bioaccumulates in macrophages leads to very few signs of toxicity even at 100 μM (23). Indeed, in spite of its massive accumulation in the liver, the hepatotoxicity of CFZ in mice and human patients has not been a significant concern (45–47). Like humans, mice treated with therapeutic CFZ doses (10 mg/kg/day) did not show signs of deteriorated health. In fact, the CFZ-induced reduction of heart rate could be linked with increased longevity in mice (48). Also, hypothermia, which is most often used as an indicator of drug toxicity in mice (49), was not seen in 8-week-CFZ-treated mice.

Regarding the therapeutic implications of these results, CFZ has proven to be highly effective for treating leprosy and active against a broad range of Gram-positive bacteria strains (*Staphylococcus*, *Streptococcus*, *Bacillus*, and *Listeria* spp.) (50) and even against drug-resistant *Staphylococcus aureus* clinical isolates that are methicillin resistant (MRSA) and vancomycin intermediate resistant (VISA) (51). Indeed, CFZ has been clinically used since the 1960s and has helped cure over 16 million leprosy patients. Many of these microorganisms tend to infect and reside within macrophages. Interestingly, chemical analysis of CFZ biocrystals has revealed that they are composed of protonated hydrochloride salt of CFZ (CFZ-HCl) within membrane-bound intracellular compartments (9). Therefore, the bioaccumulation of CFZ biocrystals in macrophages could serve to maximize the therapeutic efficacy of CFZ without significant side effects. Accordingly, it may be possible to reformulate CFZ as injectable micro- or nanocrystals to specifically target macrophages at sites of infection. Targeted local delivery could maximize CFZ benefit as a therapeutic agent while minimizing the systemic side effects that have curtailed the more widespread use of CFZ.

Considering possible signal transduction mechanisms underlying the anti-inflammatory activity of CFZ biocrystals, the cellular integrated stress response pathway is a candidate (52, 53). Although soluble CFZ can cause membrane destabilization and cell death at high concentrations (54), lower concentrations of CFZ lead to accumulation within intracellular compartments. Previously, we observed that CFZ biocrystals can also be phagocytosed by macrophages, where they are stable inside low-pH (4, 5) and counterion (Cl^-)-containing (9) membrane-bound compartments. As a weakly basic lysosomotropic drug, CFZ is prone to pH-dependent ion trapping in lysosomes and could therefore activate transcription factor EB (TFEB [55]), a master transcription factor of lysosomal biogenesis and homeostasis (56–58). In turn, this could attenuate inflammasome activation pathways and IL-1β processing (59). Alternatively, like intracellular protein aggregates and other crystalline inclusions that form in the endoplasmic reticulum (60), CFZ biocrystals may activate the unfolded protein response pathway, which could lead to downstream effects on inflammatory signaling (61, 62).

Our experiments indicate that CFZ biocrystals induce a considerable upregulation of IL-1RA production without triggering proinflammatory signaling. Since the evidence points to IL-1RA mediating the anti-inflammatory effects downstream of CFZ bioaccumulation in macrophages, future experiments aimed at elucidating the signaling pathway leading from CFZ biocrystals to IL-1RA expression should reveal further mechanistic details about the mechanism of action of CFZ and perhaps serve as the starting point for the development of new kinds of anti-inflammatory drugs. Thus, the present study strongly warrants further investigation into the mechanisms and therapeutic potential of CFZ for treating inflammatory and infectious diseases in humans. To conclude, CFZ biocrystal accumulation in macrophages could be triggering a previously unknown anti-inflammatory/immunomodulatory signaling pathway(s) of potential therapeutic value.

ACKNOWLEDGMENTS

We thank Jean Nemzek (Medical School, University of Michigan) and Pathology Cores for Animal Research at the University of Michigan for histological support and Avery Lui for help with image analysis.

G.R.R. is a consultant for Bristol-Myers Squib. The other authors have no conflicts of interest.

This study was supported by the National Institute of General Medical Sciences (NIGMS; R01GM078200 to G.R.R.), an MICHR B-to-B Pilot Seed grant (R.K.K., G.R.R.), and the University of Michigan MCubed Initiative (http://mcubed.umich.edu/). The contents of this report are solely the responsibility of the authors and do not necessarily represent the official views of the NIGMS or the National Institutes of Health.

FUNDING INFORMATION

This work, including the efforts of Gus R. Rosania, was funded by HHS | NIH | National Institute of General Medical Sciences (NIGMS) (R01GM078200). This work, including the efforts of Theodore Standiford, Kathleen A. Stringer, and Gus R. Rosania, was funded by University of Michigan (U-M) (MCubed). This work, including the efforts of Rahul K. Keswani and Gus R. Rosania, was funded by U-M | Michigan Institute for Clinical and Health Research (MICHR) (Pilot Grant).

REFERENCES

1. **Barry VC, Belton JG, Conalty ML, Denney JM, Edward DW, O'Sullivan JF, Twomey D, Winder F.** 1957. A new series of phenazines (riminocompounds) with high antituberculosis activity. Nature **179:**1013–1015. http://dx.doi.org/10.1038/1791013a0.
2. **Cholo MC, Steel HC, Fourie PB, Germishuizen WA, Anderson R.** 2012. Clofazimine: current status and future prospects. J Antimicrob Chemother **67:**290–298. http://dx.doi.org/10.1093/jac/dkr444.
3. **Reibel F, Cambau E, Aubry A.** 2015. Update on the epidemiology, diagnosis, and treatment of leprosy. Med Mal Infect **45:**383–393. http://dx.doi.org/10.1016/j.medmal.2015.09.002.
4. **Tyagi S, Ammerman NC, Li S-Y, Adamson J, Converse PJ, Swanson RV, Almeida DV, Grosset JH.** 2015. Clofazimine shortens the duration of the first-line treatment regimen for experimental chemotherapy of tuberculosis. Proc Natl Acad Sci U S A **112:**869–874. http://dx.doi.org/10.1073/pnas.1416951112.
5. **Lechartier B, Cole ST.** 2015. Mode of action of clofazimine and combination therapy with benzothiazinones against *Mycobacterium tuberculosis*. Antimicrob Agents Chemother **59:**4457–4463. http://dx.doi.org/10.1128/AAC.00395-15.
6. **Williams K, Minkowski A, Amoabeng O, Peloquin CA, Taylor D, Andries K, Wallis RS, Mdluli KE, Nuermberger EL.** 2012. Sterilizing activities of novel combinations lacking first- and second-line drugs in a murine model of tuberculosis. Antimicrob Agents Chemother **56:**3114–3120. http://dx.doi.org/10.1128/AAC.00384-12.
7. **Banerjee DK, Ellard GA, Gammon PT, Waters MF.** 1974. Some observations on the pharmacology of clofazimine (B663). Am J Trop Med Hyg **23:**1110–1115.
8. **Baik J, Stringer KA, Mane G, Rosania GR.** 2013. Multiscale distribution and bioaccumulation analysis of clofazimine reveals a massive immune system-mediated xenobiotic sequestration response. Antimicrob Agents Chemother **57:**1218–1230. http://dx.doi.org/10.1128/AAC.01731-12.
9. **Keswani RK, Baik J, Yeomans L, Hitzman C, Johnson AM, Pawate AS, Kenis PJA, Rodriguez-Hornedo N, Stringer KA, Rosania GR.** 2015. Chemical analysis of drug biocrystals: a role for counterion transport pathways in intracellular drug disposition. Mol Pharm **12:**2528–2536. http://dx.doi.org/10.1021/acs.molpharmaceut.5b00032.
10. **Harbeck RJ, Worthen GS, Lebo TD, Peloquin CA.** 1999. Clofazimine crystals in the cytoplasm of pulmonary macrophages. Ann Pharmacother **33:**250. http://dx.doi.org/10.1345/aph.18170.
11. **Sukpanichnant S, Hargrove NS, Kachintorn U, Manatsathit S, Chan-**

chairujira T, Siritanaratkul N, Akaraviputh T, Thakerngpol K. 2000. Clofazimine-induced crystal-storing histiocytosis producing chronic abdominal pain in a leprosy patient. Am J Surg Pathol **24:**129–135. http://dx.doi.org/10.1097/00000478-200001000-00016.
12. **Jadhav MV, Sathe AG, Deore SS, Patil PG, Joshi NG, Joghi NG.** 2004. Tissue concentration, systemic distribution, and toxicity of clofazimine: an autopsy study. Indian J Pathol Microbiol **47:**281–283.
13. **Tall AR, Yvan-Charvet L.** 2015. Cholesterol, inflammation and innate immunity. Nat Rev Immunol **15:**104–116. http://dx.doi.org/10.1038/nri3793.
14. **Martinon F, Pétrilli V, Mayor A, Tardivel A, Tschopp J.** 2006. Gout-associated uric acid crystals activate the NALP3 inflammasome. Nature **440:**237–241. http://dx.doi.org/10.1038/nature04516.
15. **Gehring U, Wijga AH, Brauer M, Fischer P, de Jongste JC, Kerkhof M, Oldenwening M, Smit HA, Brunekreef B.** 2010. Traffic-related air pollution and the development of asthma and allergies during the first 8 years of life. Am J Respir Crit Care Med **181:**596–603. http://dx.doi.org/10.1164/rccm.200906-0858OC.
16. **Sint T, Donohue JF, Ghio AJ.** 2008. Ambient air pollution particles and the acute exacerbation of chronic obstructive pulmonary disease. Inhal Toxicol **20:**25–29. http://dx.doi.org/10.1080/08958370701758759.
17. **Mackey JP, Barnes J.** 1974. Clofazimine in the treatment of discoid lupus erythematosus. Br J Dermatol **91:**93–96. http://dx.doi.org/10.1111/j.1365-2133.1974.tb06723.x.
18. **Lo JS, Berg RE, Tomecki KJ.** 1989. Treatment of discoid lupus erythematosus. Int J Dermatol **28:**497–507. http://dx.doi.org/10.1111/j.1365-4362.1989.tb04599.x.
19. **Chuaprapaisilp T, Piamphongsant T.** 1978. Treatment of pustular psoriasis with clofazimine. Br J Dermatol **99:**303–305. http://dx.doi.org/10.1111/j.1365-2133.1978.tb02001.x.
20. **Podmore P, Burrows D.** 1986. Clofazimine: an effective treatment for Melkersson-Rosenthal syndrome or Miescher's cheilitis. Clin Exp Dermatol **11:**173–178. http://dx.doi.org/10.1111/j.1365-2230.1986.tb00443.x.
21. **Medeiros Bezerra EL, Pereira Vilar MJ, Da Trindade Neto PB, Sato EI.** 2005. Double-blind, randomized, controlled clinical trial of clofazimine compared with chloroquine in patients with systemic lupus erythematosus. Arthritis Rheum **52:**3073–3078. http://dx.doi.org/10.1002/art.21358.
22. **Venkateswarlu B, Venkataramana D, Rao AV, Prabhakar MC, Reddy BM.** 1992. Role of rifampin and clofazimine ointments in the treatment of leprosy. Int J Lepr Other Mycobact Dis **60:**269–270.
23. **Yoon GS, Sud S, Keswani RK, Baik J, Standiford TJ, Stringer KA, Rosania GR.** 2015. Phagocytosed clofazimine biocrystals can modulate innate immune signaling by inhibiting TNF-α and boosting IL-1RA secretion. Mol Pharm **12:**2517–2527. http://dx.doi.org/10.1021/acs.molpharmaceut.5b00035.
24. **Baik J, Rosania GR.** 2011. Molecular imaging of intracellular drug-membrane aggregate formation. Mol Pharm **8:**1742–1749. http://dx.doi.org/10.1021/mp200101b.
25. **Otterness IG, Moore PF.** 1988. Immunochemical techniques. L. Chemotaxis and inflammation. *In* Methods enzymology. Elsevier, New York, NY.
26. **Matute-Bello G, Frevert CW, Martin TR.** 2008. Animal models of acute lung injury. Am J Physiol Lung Cell Mol Physiol **295:**L379–L399. http://dx.doi.org/10.1152/ajplung.00010.2008.
27. **Lax S, Wilson MR, Takata M, Thickett DR.** 2014. Using a noninvasive assessment of lung injury in a murine model of acute lung injury. BMJ Open Respir Res **1:**e000014. http://dx.doi.org/10.1136/bmjresp-2013-000014.
28. **Nayak S, Doerfler PA, Porvasnik SL, Cloutier DD, Khanna R, Valenzano KJ, Herzog RW, Byrne BJ.** 2014. Immune responses and hypercoagulation in ERT for Pompe disease are mutation and rhGAA dose dependent. PLoS One **9:**e98336. http://dx.doi.org/10.1371/journal.pone.0098336.
29. **Toth LA.** 2000. Defining the moribund condition as an experimental endpoint for animal research. ILAR J **41:**72–79. http://dx.doi.org/10.1093/ilar.41.2.72.
30. **Nemzek JA, Xiao H-Y, Minard AE, Bolgos GL, Remick DG.** 2004. Humane endpoints in shock research. Shock **21:**17–25. http://dx.doi.org/10.1097/00024382-200403001-00067.
31. **Baik J, Rosania GR.** 2012. Macrophages sequester clofazimine in an intracellular liquid crystal-like supramolecular organization. PLoS One **7:**e47494. http://dx.doi.org/10.1371/journal.pone.0047494.
32. **Keswani RK, Yoon GS, Sud S, Stringer KA, Rosania GR.** 2015. A far-red fluorescent probe for flow cytometry and image-based functional studies of xenobiotic sequestering macrophages. Cytometry A **87:**855–867. http://dx.doi.org/10.1002/cyto.a.22706.
33. **Duewell P, Kono H, Rayner KJ, Sirois CM, Vladimer G, Bauernfeind FG, Abela GS, Franchi L, Nuñez G, Schnurr M, Espevik T, Lien E, Fitzgerald KA, Rock KL, Moore KJ, Wright SD, Hornung V, Latz E.** 2010. NLRP3 inflammasomes are required for atherogenesis and activated by cholesterol crystals. Nature **464:**1357–1361. http://dx.doi.org/10.1038/nature08938.
34. **Ioannou GN, Haigh WG, Thorning D, Savard C.** 2013. Hepatic cholesterol crystals and crown-like structures distinguish NASH from simple steatosis. J Lipid Res **54:**1326–1334. http://dx.doi.org/10.1194/jlr.M034876.
35. **Simard J-C, Vallieres F, de Liz R, Lavastre V, Girard D.** 2015. Silver nanoparticles induce degradation of the endoplasmic reticulum stress sensor activating transcription factor-6 leading to activation of the NLRP-3 inflammasome. J Biol Chem **290:**5926–5939. http://dx.doi.org/10.1074/jbc.M114.610899.
36. **Demento SL, Eisenbarth SC, Foellmer HG, Platt C, Caplan MJ, Mark Saltzman W, Mellman I, Ledizet M, Fikrig E, Flavell RA, Fahmy TM.** 2009. Inflammasome-activating nanoparticles as modular systems for optimizing vaccine efficacy. Vaccine **27:**3013–3021. http://dx.doi.org/10.1016/j.vaccine.2009.03.034.
37. **Peeters PM, Eurlings IMJ, Perkins TN, Wouters EF, Schins RPF, Borm PJA, Drommer W, Reynaert NL, Albrecht C.** 2014. Silica-induced NLRP3 inflammasome activation in vitro and in rat lungs. Part Fibre Toxicol **11:**58. http://dx.doi.org/10.1186/s12989-014-0058-0.
38. **Gabay C, Smith MF, Eidlen D, Arend WP.** 1997. Interleukin 1 receptor antagonist (IL-1Ra) is an acute-phase protein. J Clin Invest **99:**2930–2940. http://dx.doi.org/10.1172/JCI119488.
39. **Gabay C, Gigley J, Sipe J, Arend WP, Fantuzzi G.** 2001. Production of IL-1 receptor antagonist by hepatocytes is regulated as an acute-phase protein in vivo. Eur J Immunol **31:**490–499. http://dx.doi.org/10.1002/1521-4141(200102)31:2<490::AID-IMMU490>3.0.CO;2-H.
40. **Dinarello CA, van der Meer JWM.** 2013. Treating inflammation by blocking interleukin-1 in humans. Semin Immunol **25:**469–484. http://dx.doi.org/10.1016/j.smim.2013.10.008.
41. **Arend WP.** 2002. The balance between IL-1 and IL-1Ra in disease. Cytokine Growth Factor Rev **13:**323–340. http://dx.doi.org/10.1016/S1359-6101(02)00020-5.
42. **McDougall AC, Horsfall WR, Hede JE, Chaplin AJ.** 1980. Splenic infarction and tissue accumulation of crystals associated with the use of clofazimine (Lamprene; B663) in the treatment of pyoderma gangrenosum. Br J Dermatol **102:**227–230. http://dx.doi.org/10.1111/j.1365-2133.1980.tb05697.x.
43. **Shi Y, Mucsi AD, Ng G.** 2010. Monosodium urate crystals in inflammation and immunity. Immunol Rev **233:**203–217. http://dx.doi.org/10.1111/j.0105-2896.2009.00851.x.
44. **Riteau N, Baron L, Villeret B, Guillou N, Savigny F, Ryffel B, Rassendren F, Le Bert M, Gombault A, Couillin I.** 2012. ATP release and purinergic signaling: a common pathway for particle-mediated inflammasome activation. Cell Death Dis **3:**e403. http://dx.doi.org/10.1038/cddis.2012.144.
45. **Bulakh PM, Kowale CN, Ranade SM, Burte NP, Chandorkar AG.** 1983. The effect of clofazimine on liver function tests in lepra reaction (ENL). Lepr India **55:**714–718.
46. **Cariello PF, Kwak EJ, Abdel-Massih RC, Silveira FP.** 2015. Safety and tolerability of clofazimine as salvage therapy for atypical mycobacterial infection in solid organ transplant recipients. Transpl Infect Dis **17:**111–118. http://dx.doi.org/10.1111/tid.12340.
47. **Kaluarachchi SI, Fernandopulle BM, Gunawardane BP.** 2001. Hepatic and haematological adverse reactions associated with the use of multidrug therapy in leprosy: a five year retrospective study. Indian J Lepr **73:**121–129.
48. **Gent S, Kleinbongard P, Dammann P, Neuhäuser M, Heusch G.** 2015. Heart rate reduction and longevity in mice. Basic Res Cardiol **110:**2. http://dx.doi.org/10.1007/s00395-014-0460-7.
49. **Stokes WS.** 2002. Humane endpoints for laboratory animals used in regulatory testing. ILAR J **43**(Suppl)**:**S31–S38.
50. **Van Rensburg CE, Jooné GK, O'Sullivan JF, Anderson R.** 1992. Antimicrobial activities of clofazimine and B669 are mediated by lysophospholipids. Antimicrob Agents Chemother **36:**2729–2735. http://dx.doi.org/10.1128/AAC.36.12.2729.
51. **Oliva B, O'Neill AJ, Miller K, Stubbings W, Chopra I.** 2004. Anti-staphylococcal activity and mode of action of clofazimine. J Antimicrob Chemother **53:**435–440. http://dx.doi.org/10.1093/jac/dkh114.

52. **Fulda S, Gorman AM, Hori O, Samali A.** 2010. Cellular stress responses: cell survival and cell death. Int J Cell Biol **2010:**214074.
53. **Kroemer G, Mariño G, Levine B.** 2010. Autophagy and the integrated stress response. Mol Cell **40:**280–293. http://dx.doi.org/10.1016/j.molcel.2010.09.023.
54. **Fukutomi Y, Maeda Y, Makino M.** 2011. Apoptosis-inducing activity of clofazimine in macrophages. Antimicrob Agents Chemother **55:**4000–4005. http://dx.doi.org/10.1128/AAC.00434-11.
55. **Sardiello M, Palmieri M, di Ronza A, Medina DL, Valenza M, Gennarino VA, Di Malta C, Donaudy F, Embrione V, Polishchuk RS, Banfi S, Parenti G, Cattaneo E, Ballabio A.** 2009. A gene network regulating lysosomal biogenesis and function. Science **325:**473–477. http://dx.doi.org/10.1126/science.1174447.
56. **Logan R, Kong AC, Krise JP.** 2014. Time-dependent effects of hydrophobic amine-containing drugs on lysosome structure and biogenesis in cultured human fibroblasts. J Pharm Sci **103:**3287–3296. http://dx.doi.org/10.1002/jps.24087.
57. **Parks A, Charest-Morin X, Boivin-Welch M, Bouthillier J, Marceau F.** 2015. Autophagic flux inhibition and lysosomogenesis ensuing cellular capture and retention of the cationic drug quinacrine in murine models. PeerJ **3:**e1314. http://dx.doi.org/10.7717/peerj.1314.
58. **Zhitomirsky B, Assaraf YG.** 2015. Lysosomal sequestration of hydrophobic weak base chemotherapeutics triggers lysosomal biogenesis and lysosome-dependent cancer multidrug resistance. Oncotarget **6:**1143–1156. http://dx.doi.org/10.18632/oncotarget.2732.
59. **Emanuel R, Sergin I, Bhattacharya S, Turner JN, Epelman S, Settembre C, Diwan A, Ballabio A, Razani B.** 2014. Induction of lysosomal biogenesis in atherosclerotic macrophages can rescue lipid-induced lysosomal dysfunction and downstream sequelae. Arterioscler Thromb Vasc Biol **34:**1942–1952. http://dx.doi.org/10.1161/ATVBAHA.114.303342.
60. **Hasegawa H.** 2013. Aggregates, crystals, gels, and amyloids: intracellular and extracellular phenotypes at the crossroads of immunoglobulin physicochemical property and cell physiology. Int J Cell Biol **2013:**604867.
61. **Hasegawa H, Wendling J, He F, Trilisky E, Stevenson R, Franey H, Kinderman F, Li G, Piedmonte DM, Osslund T, Shen M, Ketchem RR.** 2011. In vivo crystallization of human IgG in the endoplasmic reticulum of engineered Chinese hamster ovary (CHO) cells. J Biol Chem **286:**19917–19931. http://dx.doi.org/10.1074/jbc.M110.204362.
62. **Bettigole SE, Glimcher LH.** 2015. Endoplasmic reticulum stress in immunity. Annu Rev Immunol **33:**107–138. http://dx.doi.org/10.1146/annurev-immunol-032414-112116.